HHS Public Access

Author manuscript

*ACS Chem Biol*. Author manuscript; available in PMC 2018 May 19.

Published in final edited form as:

*ACS Chem Biol*. 2017 May 19; 12(5): 1327–1334. doi:10.1021/acschembio.6b01066.

# Single Particle Observation of SV40 VP1 Polyanion-Induced Assembly Shows that Substrate Size and Structure Modulate Capsid Geometry

**Chenglei Li**[1,*], **Andrew R. Kneller**[2,*], **Stephen C. Jacobson**[2,†], and **Adam Zlotnick**[1,†]

[1]Department of Molecular and Cellular Biochemistry, Indiana University, Bloomington, Indiana, 47405, USA

[2]Department of Chemistry, Indiana University, Bloomington, Indiana, 47405, USA

## Abstract

Simian virus 40 capsid protein (VP1) is a unique system for studying substrate-dependent assembly of a nanoparticle. Here, we investigate a simplest case of this system where 12 VP1 pentamers and a single polyanion, e.g. RNA, form a T=1 particle. To test the roles of polyanion substrate length and structure during assembly, we characterized the assembly products with size exclusion chromatography, transmission electron microscopy, and single-particle resistive-pulse sensing. We found that 500 and 600 nt RNAs had the optimal length and structure for assembly of uniform T=1 particles. Longer 800 nt RNA, shorter 300 nt RNA, and a linear 600 unit poly(styrene sulfonate) (PSS) polyelectrolyte produced heterogeneous populations of products. This result was surprising as the 600mer PSS and 500 nt RNA have similar mass and charge. Like ssRNA, PSS also has a short 4 nm persistence length, but unlike RNA, PSS lacks a compact tertiary structure. These data indicate that even for flexible substrates, shape as well as size affect assembly and are consistent with the hypothesis that work, derived from protein-protein and protein-substrate interactions, is used to compact the substrate.

### Keywords

Simian virus 40; capsid assembly; RNA packaging; polyelectrolyte; single particle; nanofluidics; resistive-pulse sensing

Many single-stranded RNA (ssRNA) viruses are able to spontaneously assemble and concomitantly package their genomes or other anionic substrates [1–6]. Identifying the factors that modulate packaging could shed light on new antiviral targets and promote reengineering of capsid proteins (CPs) or nucleic acids (NAs) for gene therapy, drug delivery, and other applications.

To consider the complexity of capsid assembly with ssRNA, a reductionist approach is necessary. In many cases, successful assembly requires a concerted interplay between the size and structure of ssRNA and the spontaneous curvature of the growing capsid [7–9].

*Co-first authors

†co-submitting authors.

Electrostatic interactions between positive charges on CPs and negative charges on RNA provide an important thermodynamic driving force for this process [10–13]. Therefore, focusing on the length and structure of RNA substrates provides an informative start for a better understanding of the packaging mechanism [5, 6].

To characterize the roles of the length and structure of RNA on assembly requires a simple yet easily manipulated in vitro assembly system. Simian virus 40 (SV40) is an attractive candidate. SV40 is a small, nonenveloped double-stranded DNA (dsDNA) virus belonging to the polyomavirus family. In vivo, SV40 forms a 45 nm diameter capsid of 72 VP1 pentamers around its 5200 bp dsDNA genome, which is compacted by bound histones [14, 15]. Mimicking ssRNA viruses, VP1 pentamer can bind nucleic acid via a C-terminal tail rich in basic amino acids, which extends into the center of the virion and is typically unresolved in crystallographic maps [14, 16–18]. In vitro, SV40, and other polyomaviruses, VP1 pentamers can assemble into a broad array of structures from 20 nm T=1 capsids to 40 nm T=7 capsids to 40 nm diameter tubes [19, 20]. Different nucleic acid substrates yield a similar range of structures with relatively stiff dsDNA favoring T=7 particles [21, 22]. On ssRNA substrates, VP1 forms uniform 22 nm diameter T=1 virus-like particles (VLPs) under mild solution conditions (50 mM MOPS, pH 7.2, 125 mM NaCl) in the absence of cellular or external factors [23]. Recent studies on Cowpea Chlorotic Mottle Virus (CCMV) demonstrated how different RNA sizes affect the capsid geometry and assembly efficiency [24–26]. However, CCMV is assembled from 90 dimers and may follow a complex assembly path to generate the mixture of pentameric and hexameric vertices found in a T=3 icosahedron [6, 27]. Conversely, a dodecahedral nucleoprotein complex is small enough that a rigorous molecular dynamics study including protein and RNA components can be calculated [12, 13]. Therefore, a dodecahedral assembly system is extremely attractive as a simple and robust model for characterizing the effects of substrate length and structure.

Evaluating assembly on different substrates with various lengths and structures requires multiple techniques. Here, we use size exclusion chromatography (SEC), transmission electron microscopy (TEM), and single-particle resistive-pulse sensing. SEC can be used to assess the size distribution of large populations of particles but lacks detail [23, 27–29]. Negative stain TEM allows visualization of individual particles but can cause distortion and may not show a representative sample. Resistive-pulse sensing is a nondestructive technique for rapid-sensing, characterization, and sorting of particles with nanometer dimensions [30–33]. This technique measures changes in ion current resulting from displacement of an electrolyte solution by a solute as it passes through one or several nanopores. The amplitude of the pulse is proportional to the volume of solute displaced [34], and the frequency is proportional to particle concentration. Resistive-pulse sensing has been used to characterize Hepatitis B Virus assembly [30, 35–37].

To investigate the role of substrate on capsid assembly, we tried to select substrates that matched the simplicity of the dodecahedral capsid. For SV40, each VP1 monomer has 5 positive charges on the C-terminal tail, resulting in a total of 300 positive charges for a T=1 VLP. Thus, we chose four lengths of RNA with 300, 500, 600, and 800 nucleotides (nt). A linear poly(styrene sulfonate) (PSS) molecule with an average length of 600 subunits was also selected to make a head-to-head comparison to test whether substrate structure affects

assembly. We wished to maximize the difference between characteristics of our RNA substrates and the PSS comparator. PSS has a persistence length similar to that of a hypothetical ssRNA that lacks base-pairs but PSS has a smaller excluded volume due to the hydrophobic styrene side chains [38]. Conversely viral RNA, in general, has a pronounced tendency to form compact structures based on its density of base-pairing [39, 40], thus our source of RNA is the P1 region of Bovine Enterovirus [41]. We found the particle yield and uniformity were sensitive to both substrate length and structure.

## Results

### Assembly on RNA and Polyelectrolyte with Various Lengths

SV40 VP1 pentamers can assemble on nucleic acid (NA) in vitro into various structures governed by protein-protein interactions and the nature of the NA scaffold [22]. The ratio of VP1 pentamer to NA dictated assembly products; assembly on a linear 600 bp dsDNA led to the formation of 22 and 45 nm diameter particles and even tubular structures [22]. By contrast, assembly on a flexible ssRNA molecule of similar size, 500 nt, yielded uniform 22 nm diameter T=1 virus-like particles (VLPs) [23]. These results suggested that NA length and structure modulate the size and geometry of assembly products.

To further investigate the effect of NA length on assembly, we synthesized viral RNAs with lengths of 300, 500, 600, and 800 nt. As ssRNA molecules (except some homopolymers such as polyA) have substantial high-order structure due to base-pairing, we also examined assembly on PSS with an average length of 600 units; PSS is a flexible, linear polyanion without secondary structures.

To assemble a dodecahedral capsid with one polyanionic cargo, VP1 pentamers were mixed with RNA or PSS at a molar ratio of 12:1; the final assembly buffer was 50 mM MOPS, pH 7.2, 125 mM NaCl, a condition previously examined[42]. Using dynamic light scattering, we found changing ionic strength had little effect on the assembly products for a given substrate; thus, ionic strength was not further investigated. Mixtures were allowed to equilibrate for 0.5 h at room temperature (22C) and then evaluated by SEC (Figure 1). Assembly with different substrates resulted in different elution profiles. All RNA assembly products had symmetrical peaks, which suggests a largely homogeneous population. However, the elution volumes were different with 10.1, 9.3, 9.2, and 9 mL for 300, 500, 600, and 800 nt RNA, respectively. This difference in elution volumes indicated that 300 nt RNA assembly products may have either fewer subunits or more compact conformation, whereas 800 nt RNA assembly products may be larger than previously characterized T=1 VLPs. In contrast, PSS assembly products eluted as a major peak centered at 9 mL with a shoulder at ~7.9 mL. This elution profile suggested that the majority of PSS assembly products had a similar size distribution as the 800 nt RNA assembly products, but a portion were larger than T=1 VLPs. There was no evidence of incomplete particles in any of these assembly reactions. These results for both 500 nt and 600 nt RNAs were consistent with our earlier studies with the 500 nt RNA, in which one substrate molecule was packaged for each particle, and the association energy was relatively strong [42].

As seen in Figure 1, the shorter RNA substrates (300 nt) with fewer negative charges had more free pentamers remaining after assembly compared to 500 nt RNA substrates. In contrast, the longer RNA (800 nt) substrates had less free pentamers remaining. On the basis of absorbance of protein and RNA, we quantified the percentage of VP1 in the capsid and pentamer SEC peaks which allowed us to calculate the average number of substrates per capsid (Table 1). For the 300 nt RNA, 77% of the VP1 was in the capsid peak resulting in an average of 1.30 RNA molecules per capsid. That is, about 3/4 of the capsids contained a single RNA.

## Morphologies of Assembled Products

RNA and PSS assembly products were also examined by transmission electron microscopy (TEM) (Figure 2). As expected, 500 nt RNA assembly products showed T=1 size spherical particles with diameters of 22 nm (Figure 2B). In contrast to the slight size difference shown by SEC, 300 nt RNA assembly products displayed sizes similar to T=1 VLPs with diameters of 22 nm (Figure 2A) although size differences obscured by staining could not be ruled out. The majority of 800 nt RNA assembly products had sizes similar to T=1 VLPs (Figure 2C), but larger nonspherical particles were observed (Figure 2C, highlighted by white circles). As a working hypothesis, each capsid is nucleated by a single event. As there is no reason to suspect heterogeneous nucleation where a complete capsid could stimulate formation of an adjacent complex, a doublet or triplet comprised of abutting capsids may result in cases where assembly is initiated at multiple sites on a single RNA molecule. We note that the larger numbers of pentamers can compensate for the negative charges on the longer substrate. This hypothesis is also consistent with strong RNA-pentamer and pentamer-pentamer interactions that render the nucleated complex unable to correct itself to anneal into T=1 VLPs.

PSS assembly products showed strikingly different morphologies (Figure 2D) from RNA assembly products. Approximately 40% of the particles were T=1 like particles, 50% of the particles were doublets (two 22 nm particles connected together), and 10% of the particles were triplets (three particles connected together in a linear or compact fashion). We note that PSS is a linear polyanion without secondary structure, whereas the secondary structure of ssRNA makes it more compact and better represented physically as a branched polymer [39]. For PSS the length of the linear molecule was enough to allow nucleation at multiple sites and formation of separated particles, in comparison with more compact 800 nt RNA assembled nonspherical particles (Figure 2C and D).

## Resistive-Pulse Measurements of RNA and PSS Assembly Products

Resistive-pulse sensing was used to characterize the populations of RNA and PSS assembly products. The use of multiple nanopores in series increases measurement precision and improves statistics compared to a single nanopore device [43]. The dimensions of the nanopores were tailored to sense SV40 T=1 VLP and also accommodate larger species; consequently, the nanopores were milled 70 nm wide, 70 nm deep, and 290 nm long.

To improve measurement precision of these nucleoprotein complexes, we used nanofluidic devices with four pores in series. Also, to work at the relatively low ionic strengths (350 mM

NaCl) used in these experiments, the glass surface of the device was coated with a short-chain poly(ethylene glycol) to minimize capsid-surface interactions and to suppress electro-osmotic flow [30].

Samples for resistive-pulse measurements were RNA and PSS assembly products fractionated into 0.5 mL aliquots by SEC with a Superose 6 column. Figure 3 shows histograms of the average pulse amplitude for selected fractions for each of the four assembly substrates. For 300 nt RNA assembly (Figure 3A), fraction 21 was collected from the center of the peak (10.1 mL; green line in Figure 1). The symmetrical distributions shown for different fractions suggest a homogeneous population for 300 nt RNA assembly products, consistent with SEC (Figure 1) and TEM (Figure 2A). For 500 nt RNA assembly (Figure 3B), fraction 20 was collected from the center of the peak (9.3 mL; blue line in Figure 1). Resistive-pulse measurements showed that other fractions are largely homogeneous with a few larger species observed in an early fraction (fraction 17). Of note, the 300 nt and 500 nt RNA T=1 capsids displace approximately the same volume of electrolyte indicating that they are the same size, in contrast to the SEC results (Figure 1) but consistent with TEM results (Figure 2).

The histograms of 800 nt RNA assembly clearly show the formation of heterogeneous particles (Figure 3C). Fraction 19, collected from the center of the SEC peak (red line in Figure 1), were almost entirely T=1 VLPs. However, the earlier fraction 16 showed a significant number of pulses with amplitudes ($\Delta i/i$ = 0.40) nearly double the amplitude of the T=1 VLP ($\Delta i/i$ = 0.22). This result indicates that these particles contain approximately twice the protein volume of a T=1 capsid and are consistent with the oval-shaped particles obvious by TEM (Figure 2C, white circles).

The overlay of PSS assembly fractions is a more complex story (Figure 3D). Fractions 19 and 21, collected from the center and the tail of the SEC peak, respectively, are dominated by T=1 particles but are surprisingly broad. The high mass shoulder of the SEC peak (7.9 mL), fractions 15 and 17, included ill-resolved larger species. These data are consistent with the doublets and triplets observed by TEM (Figure 2D) but also suggest a much greater degree of heterogeneity than observed in the TEM micrographs.

To directly visualize the size differences among substrates, histograms of fractions collected at the same elution volume are overlaid in Figure 4. The histogram overlay of fraction 17 (Figure 4A), the high molecular weight edge of the SEC peak, shows that the assembly becomes more heterogeneous as the size of an RNA substrate increases. However, PSS, which is smaller than the 800 nt RNA, shows the most heterogeneous distribution with a continuum of pulse amplitudes. This observation is in contrast with the distinct peaks for VLP doublets and triplets seen in early fractions with the 800 nt RNA assembly products (Figure 3C). For all substrates, particles isolated from the center of the SEC peak are homogeneous with the majority population at the T=1 size (Figure 4B). Particles from the trailing edge of the SEC peak (fraction 21) are largely homogeneous, except for PSS. Again, PSS assembly produced a wide range of products, this time at lower $\Delta i/i$ values, indicating sizes smaller than T=1 VLP. These smaller particles may be incomplete or have diameters less than 22 nm (Figure 2D).

Figure 5 shows histograms of the pore-to-pore times for products assembled with 300 nt RNA, 500 nt RNA, 800 nt RNA, and 600mer PSS and, subsequently, purified by SEC. The pore-to-pore times were measured between adjacent current pulses for a single particle. With four pores in series, three pore-to-pore times were averaged for each series of pulses from a VLP translocating the series of pores. For these measurements, the VLPs are negatively charged and migrating electrophoretically in the anodic direction (i.e., toward the positive electrode). For VLPs assembled with RNA, pore-to-pore times decrease with increasing RNA length. Excess negative charge from the RNA contributes significantly to the shift toward higher electrophoretic mobilities of the particles. Products assembled with PSS have the shortest pore-to-pore times (i.e., highest electrophoretic mobilities), which indicate these VLPs have the largest amount of excess negative charge exposed and contributing to the electrophoretic mobility.

## Discussion

We have shown that the length and structure of substrates affect the assembly of SV40 T=1 VLPs. The optimal substrate is determined by a complex interplay between capsid charge, capsid size, and substrate length and structure. Shorter substrates yield more compact particles, and longer substrates yield oversized particles. These observations are consistent with the hypothesis that the capsid proteins may have to drive the substrate to an ideal conformation and, conversely, that assembly may be supported by an ideal shape [8, 9].

In our model system, we found that the secondary and tertiary structure of cargos modulate assembly. The 600mer PSS and 500 nt RNA have a similar charge but dissimilar assembly products. This difference indicates that the electrostatic interactions alone were not able to compensate for energetic cost, work, required to condense the substrate. The structure inherent in RNA led to a more compact molecule[39] and greatly reduced the barrier for successful assembly of a compact capsid. In general, viral RNA is substantially more compact than nonviral sequences; Gopal and co-workers observed that large RNAs formed ellipsoidal structures. The hydrodynamic radius, $R_h$, of a nonviral RNA was about half the radius of gyration one would calculate based on its length, and the $R_h$ for nonviral RNA was as much as twice that of viral RNA [39, 40]. Our data support the concept that compactness matters. Similarly, model studies with gold nanoparticles show that there is an optimal size for capsid assembly [4, 8, 44]. The longer RNA and PSS frequently lead to doublets and triplets of capsids. Doublets and triplets may be kinetic traps because they do not readily equilibrate into a T=1 capsid. However, we cannot unequivocally differentiate whether singlets, doublets, triplets, or a mixture represent the energy minimum for this reaction.

Tresset and co-workers found that CCMV had a preference for PSS over ssRNA [38] whereas we find that SV40 T=1 binds both substrates with high affinity but forms more uniform particles on RNA. In these two systems, CCMV and SV40, the electrostatic character of interaction is very similar. One possible basis for the difference in substrate preference is rooted in the mechanism of assembly. CCMV assembly appears to depend on initial formation of a nonicosahedral nucleoprotein complex that eventually anneals into a capsid [5, 6, 26]. For SV40, in a SAXS study, assembly on RNA appeared to be a two-state reaction with no large diameter intermediates observed [42]. The differences in these

mechanisms are likely to arise from the strength of protein-protein interactions relative to protein-RNA interactions, with stronger protein-protein interactions favoring the two-state mechanism [6, 13, 26, 45]. Conversely, weak protein-protein interactions will favor initial formation of an amorphous nucleoprotein complex and are more compatible with a large unstructured substrate such as PSS. Strong protein-protein interactions will favor stepwise addition of subunits to a geometrically regular complex and are better suited for a more compact substrate, exemplified by viral RNA. We note that the kinetics of protein-protein interaction, which will also be modulated by substrate shape, will contribute to the choice of paths.

'Overcharged' capsids, where the negative charge of the substrate exceeds the positive charge on capsid, appear to be thermodynamically favored [12, 46, 47]. In general, assembly around NAs is predominantly driven by electrostatic interactions between NA phosphate groups and basic amino acids. The typical 'charge ratio' of negative charge on NAs to the positive charge on the protein is estimated to be ~1.5:1 for many ssRNA viruses [12, 46, 47]. However, recent theoretical models based on linear polyelectrolytes predicted that optimal NA charge may be equal to positive capsid charges [13, 48–50]. This contradiction is mainly due to the structural differences between ssRNA and polyelectrolytes, which suggests that NA tertiary structure plays more decisive roles than charges alone [12].

To better understand the effect of charges on SV40 T=1 assembly, the charge ratios of negative charge on five substrates to the positive charge on 12 pentamers are listed in Table 2, assuming each VP1 contains five positively charged residues that interact with the substrate. The calculated ratio indicates that capsid assembly led to spontaneous 'overcharging'; that is, the negative charge of the substrate exceeds the positive charge on the capsid. We found that charge ratios of 1 and 1.67 gave the highest yield of T=1 VLPs. Interestingly, the 300 nt RNA, the number of RNA molecules per capsid is 1.3 (Table 1), consistent with a situation where 77% of capsids have one RNA and a charge ratio of 1 and 23% of capsids have two 300 nt RNAs and a charge ratio of 2 (Table 2). For PSS, the charge ratio is 2, within the reported optimal ratio range [11, 12, 46, 47], though this ratio produced a substantial percentage of malformed particles. The highest charge ratio tested in our study was 2.67 for 800 nt RNA, which produced T=1 VLPs, but predictably led to malformed, oversized particles. The results with RNA were largely consistent with the conclusions from a recent report which used coarse-grained models based on experimental observations [12]. However, the effect of PSS on assembly shows that even in a supposedly simple system, the products of assembly can be diverse. The degree of overcharging is also seen in the pore-to-pore times in Figure 5. As the RNAs increase in length, the pore-to-pore times decrease. These results are consistent with the charge ratio calculated in Table 2. Interestingly, products assembled with PSS showed the shortest pore-to-pore times. These VLPs most likely do not have the PSS completely packaged inside the particle; consequently, excess charge dangling outside the VLPs contributes to a greater extent to the electrophoretic mobility than expected from the calculated charge ratio.

## Materials and Methods

### Protein and Substrate for Assembly Reactions

SV40 VP1 VLPs and pentamers were produced in Spodoptera frugiperda 9 (Sf9) insect cells as previously described [51]. Pentamers were obtained by dissociating VLPs by dialysis first against 20 mM Tris-Cl, pH 8.9, 50 mM NaCl, 2 mM DTT (dissociation buffer) with 5 mM EDTA and then against dissociation buffer with 2 mM EDTA at 4 °C. The dialysate was centrifuged at 20,000 g for 30 min at and 4 °C to sediment aggregated protein. The clarified supernatant was loaded on a Superose 6 column equilibrated in 2x assembly buffer (100 mM MOPS, pH 7.2, 250 mM NaCl), and the pentamer peak was pooled and quantified by UV absorbance with an extinction coefficient of $\varepsilon_{280}$ = 32,890 $M^{-1}cm^{-1}$ per VP1 monomer [22].

PSS with MW = 126,700 Da was purchased from Scientific Polymer Products. The 300, 500, 600, and 800 nt RNAs were in vitro transcribed from linearized pUC19-BEV-1 with a MegaScript T7 kit (Ambion).

### Equilibrated Assembly Reactions

VP1 pentamers (3.6 μM) purified by Superose 6 column were mixed with 0.3 μM RNA or PSS in 2x assembly buffer. SEC was performed with a Superose 6 column (22 mL, GE Healthcare) equilibrated with assembly buffer. Samples for TEM were adsorbed to freshly glow-discharged, formvar-carbon coated copper grids (EM sciences) for 25 s, stained with 2% uranyl acetate for 25 s, and washed with deionized water. Samples were visualized with a JEOL JEM 1010.

### Resistive-Pulse Device Fabrication and Measurement

Nanofluidic devices were fabricated as previously described [36]. The microchannels were formed in D263 glass substrates by standard UV photolithography and wet chemical etching. The nanochannels and nanopores were milled directly into the glass substrates with a dual-beam focused ion beam (FIB) instrument (Auriga 60, Carl Zeiss, GmbH) controlled by NanoPatterning and Visualization Engine (NPVE; FIBICS, Inc.). Nanopores for VLP measurements were typically 70 ± 5 nm wide, 70 ± 5 nm deep, and 290 ± 10 nm long. The pore-to-pore channels formed between pores were 310 ± 10 nm wide, 120 ± 5 nm deep and 520 ± 10 nm long. The two nanochannel sections that connect the pores at the ends to the microchannels were milled 520 ± 10 nm wide and 225 ± 5 nm deep. Device dimensions were determined by SEM and AFM (MFP-3D, Asylum Research, Inc.).

Channels were sequentially filled with methanol, 50:50 methanol:water, water, 0.1 M NaOH, water, and 50 mM MOPS buffer (pH 7.5) with 350 mM NaCl. Prior to sensing the SV40 particles assembled with PSS and RNA, the channels were coated with (2-[methoxypoly(ethyleneoxy)6-9propyl] dimethylmethoxysilane) to reduce electroosmotic flow and minimize particle adsorption. All solutions were filtered with 20 nm syringe filters. Ag/AgCl electrodes were placed inside the buffer-filled reservoirs, and an Axopatch 200B current amplifier (Molecular Devices, Inc.) was used to apply the potential and to measure the current. Collection frequencies of 100 kHz and filter frequencies of 10 kHz were used for the sensing experiments.

Current data were imported into MATLAB (MathWorks) and analyzed with a modified version of OpenNanopore [52] to determine pulse amplitude (Δi), baseline current adjacent to each pulse (i), pore-to-pore time ($t_{pp}$), and pulse width (w) for each capsid that transits the four pores in series.

## Acknowledgments

We thank A Oppenheim for starting us on the line of research. We thank J C-Y Wang and C Schlicksup for help with collecting TEM images L Lee for assistance with analyzing chromatography data. Electron microscopy was performed at the Indiana University (IU) Electron Microscopy Center, and FIB milling and SEM analysis were performed in the IU Nanoscale Characterization Facility.

This work was supported in part by NSF grant CHE-1308484 to SCJ and NIH grant R03-AI102873 to AZ.

## References

1. Fraenkel-Conrat H, Williams RC. Reconstitution of Active Tobacco Mosaic Virus from Its Inactive Protein and Nucleic Acid Components. Proc Natl Acad Sci U S A. 1955; 41:690–698. [PubMed: 16589730]
2. Bancroft JB, Hiebert E. Formation of an infectious nucleoprotein from protein and nucleic acid isolated from a small spherical virus. Virology. 1967; 32:354–356. [PubMed: 6025882]
3. Krol MA, Olson NH, Tate J, Johnson JE, Baker TS, Ahlquist P. RNA-controlled polymorphism in the in vivo assembly of 180-subunit and 120-subunit virions from a single capsid protein. Proc Natl Acad Sci U S A. 1999; 96:13650–13655. [PubMed: 10570127]
4. Chen C, Kwak E-S, Stein B, Kao CC, Dragnea B. Packaging of gold particles in viral capsids. J Nanosci Nanotech. 2005; 5:2029–2033.
5. Comas-Garcia M, Garmann RF, Singaram SW, Ben-Shaul A, Knobler CM, Gelbart WM. Characterization of Viral Capsid Protein Self-Assembly around Short Single-Stranded RNA. J Phys Chem B. 2014; 118:7510–7519.
6. Garmann RF, Comas-Garcia M, Gopal A, Knobler CM, Gelbart WM. The assembly pathway of an icosahedral single-stranded RNA virus depends on the strength of inter-subunit attractions. J Mol Biol. 2014; 426:1050–1060. [PubMed: 24148696]
7. Aniagyei SE, Dufort C, Kao CC, Dragnea B. Self-assembly approaches to nanomaterial encapsulation in viral protein cages. Journal of materials chemistry. 2008; 18:3763–3774. [PubMed: 19809586]
8. He L, Porterfield Z, van der Schoot P, Zlotnick A, Dragnea B. Hepatitis virus capsid polymorph stability depends on encapsulated cargo size. ACS Nano. 2013; 7:8447–8454. [PubMed: 24010404]
9. Zlotnick A, Porterfield JZ, Wang JC. To build a virus on a nucleic acid substrate. Biophys J. 2013; 104:1595–1604. [PubMed: 23561536]
10. Garmann RF, Comas-Garcia M, Koay MS, Cornelissen JJ, Knobler CM, Gelbart WM. Role of electrostatics in the assembly pathway of a single-stranded RNA virus. J Virol. 2014; 88:10472–10479. [PubMed: 24965458]
11. Kivenson A, Hagan MF. Mechanisms of capsid assembly around a polymer. Biophys J. 2010; 99:619–628. [PubMed: 20643082]
12. Perlmutter JD, Qiao C, Hagan MF. Viral genome structures are optimal for capsid assembly. Elife. 2013; 2:e00632. [PubMed: 23795290]
13. Perlmutter JD, Perkett MR, Hagan MF. Pathways for virus assembly around nucleic acids. J Mol Biol. 2014; 426:3148–3165. [PubMed: 25036288]
14. Stehle T, Gamblin SJ, Yan Y, Harrison SC. The structure of simian virus 40 refined at 3.1 A resolution. Structure. 1996; 4:165–182. [PubMed: 8805523]
15. Imperiale, MJ., Major, EO. Polyomaviruses. In: Knipe, DM.Griffin, DE.Lamb, RA.Martin, MA.Roizman, B., Straus, SE., editors. Fields Virology. Lippincott Williams & Wilkins; Philadelphia: 2007. p. 2263-2298.

16. Fisher AJ, Johnson JE. Ordered duplex RNA controls capsid architecture in an icosahedral animal virus. Nature. 1993; 361:176–179. [PubMed: 8421524]
17. Smith TJ, Chase E, Schmidt T, Perry KL. The structure of cucumber mosaic virus and comparison to cowpea chlorotic mottle virus. J Virol. 2000; 74:7578–7586. [PubMed: 10906212]
18. Speir JA, Munshi S, Wang G, Baker TS, Johnson JE. Structures of the native and swollen forms of cowpea chlorotic mottle virus determined by X-ray crystallography and cryo-electron microscopy. Structure. 1995; 3:63–78. [PubMed: 7743132]
19. Kanesashi SN, Ishizu K, Kawano MA, Han SI, Tomita S, Watanabe H, Kataoka K, Handa H. Simian virus 40 VP1 capsid protein forms polymorphic assemblies in vitro. J Gen Virol. 2003; 84:1899–1905. [PubMed: 12810885]
20. Salunke D, Caspar DL, Garcea RL. Polymorphism in the assembly of polyomavirus capsid protein VP1. Biophys J. 1989; 56:887–900. [PubMed: 2557933]
21. Kler S, Wang JC, Dhason M, Oppenheim A, Zlotnick A. Scaffold properties are a key determinant of the size and shape of self-assembled virus-derived particles. ACS Chem Biol. 2013; 8:2753–2761. [PubMed: 24093474]
22. Mukherjee S, Kler S, Oppenheim A, Zlotnick A. Uncatalyzed assembly of spherical particles from SV40 VP1 pentamers and linear dsDNA incorporates both low and high cooperativity elements. Virology. 2010; 397:199–204. [PubMed: 19942248]
23. Kler S, Asor R, Li C, Ginsburg A, Harries D, Oppenheim A, Zlotnick A, Raviv U. RNA encapsidation by SV40-derived nanoparticles follows a rapid two-state mechanism. Journal of the American Chemical Society. 2012; 134:8823–8830. [PubMed: 22329660]
24. Comas-Garcia M, Cadena-Nava RD, Rao AL, Knobler CM, Gelbart WM. In vitro quantification of the relative packaging efficiencies of single-stranded RNA molecules by viral capsid protein. J Virol. 2012; 86:12271–12282. [PubMed: 22951822]
25. Cadena-Nava RD, Comas-Garcia M, Garmann RF, Rao AL, Knobler CM, Gelbart WM. Self-assembly of viral capsid protein and RNA molecules of different sizes: requirement for a specific high protein/RNA mass ratio. J Virol. 2012; 86:3318–3326. [PubMed: 22205731]
26. Garmann RF, Comas-Garcia M, Knobler CM, Gelbart WM. Physical Principles in the Self-Assembly of a Simple Spherical Virus. Acc Chem Res. 2016; 49:48–55. [PubMed: 26653769]
27. Johnson JM, Tang J, Nyame Y, Willits D, Young MJ, Zlotnick A. Regulating self-assembly of spherical oligomers. Nano Lett. 2005; 5:765–770. [PubMed: 15826125]
28. Li C, Wang JC, Taylor MW, Zlotnick A. In Vitro Assembly of an Empty Picornavirus Capsid follows a Dodecahedral Path. J Virol. 2012; 86:13062–13069. [PubMed: 23015694]
29. Tan Z, Pionek K, Unchwaniwala N, Maguire ML, Loeb DD, Zlotnick A. The Interface between Hepatitis B Virus Capsid Proteins Affects Self-Assembly, Pregenomic RNA Packaging, and Reverse Transcription. J Virol. 2015; 89:3275–3284. [PubMed: 25568211]
30. Zhou K, Li L, Tan Z, Zlotnick A, Jacobson SC. Characterization of hepatitis B virus capsids by resistive-pulse sensing. Journal of the American Chemical Society. 2011; 133:1618–1621. [PubMed: 21265511]
31. Howorka S, Siwy Z. Nanopore analytics: sensing of single molecules. Chem Soc Rev. 2009; 38:2360–2384. [PubMed: 19623355]
32. Luo L, German SR, Lan WJ, Holden DA, Mega TL, White HS. Resistive-pulse analysis of nanoparticles. Annu Rev Anal Chem. 2014; 7:513–535.
33. Haywood DG, Saha-Shah A, Baker LA, Jacobson SC. Fundamental studies of nanofluidics: nanopores, nanochannels, and nanopipets. Anal Chem. 2015; 87:172–187. [PubMed: 25405581]
34. Horak D, Peska J, Svec F, Stamberg J. The influence of porosity of discrete particles upon their apparent dimensions as measured by the Coulter principle. Powder Technol. 1982; 31:5.
35. Harms ZD, Mogensen KB, Nunes PS, Zhou K, Hildenbrand BW, Mitra I, Tan Z, Zlotnick A, Kutter JP, Jacobson SC. Nanofluidic devices with two pores in series for resistive-pulse sensing of single virus capsids. Anal Chem. 2011; 83:9573–9578. [PubMed: 22029283]
36. Harms ZD, Selzer L, Zlotnick A, Jacobson SC. Monitoring Assembly of Virus Capsids with Nanofluidic Devices. ACS Nano. 2015; 9:9087–9096. [PubMed: 26266555]
37. Harms ZD, Haywood DG, Kneller AR, Selzer L, Zlotnick A, Jacobson SC. Single-particle electrophoresis in nanochannels. Anal Chem. 2015; 87:699–705. [PubMed: 25489919]

38. Tresset G, Tatou M, Le Coeur C, Zeghal M, Bailleux V, Lecchi A, Brach K, Klekotko M, Porcar L. Weighing Polyelectrolytes Packaged in Viruslike Particles. Phys Rev Lett. 2014; 113:128305. [PubMed: 25279650]

39. Gopal A, Zhou ZH, Knobler CM, Gelbart WM. Visualizing large RNA molecules in solution. RNA. 2012; 18:284–299. [PubMed: 22190747]

40. Gopal A, Egecioglu DE, Yoffe AM, Ben-Shaul A, Rao AL, Knobler CM, Gelbart WM. Viral RNAs Are Unusually Compact. PLoS One. 2014; 9:e105875. [PubMed: 25188030]

41. Li C, Wang JC, Taylor MW, Zlotnick A. In vitro assembly of an empty picornavirus capsid follows a dodecahedral path. J Virol. 2012; 86:13062–13069. [PubMed: 23015694]

42. Kler S, Asor R, Li C, Ginsburg A, Harries D, Oppenheim A, Zlotnick A, Raviv U. RNA encapsidation by SV40-derived nanoparticles follows a rapid two-state mechanism. J Am Chem Soc. 2012; 134:8823–8830. [PubMed: 22329660]

43. Kondylis P, Zhou Z, Harms ZD, Kneller AR, Lee LS, Zlotnick A, Jacobson SC. Nanofluidic Devices with 8 Pores in Series for Real-Time, Resistive-Pulse Analysis of Hepatitis B Virus Capsid Assembly. Anal Chem. 2017:6b04491.

44. Goicochea NL, De M, Rotello VM, Mukhopadhyay S, Dragnea B. Core-like particles of an enveloped animal virus can self-assemble efficiently on artificial templates. Nano Lett. 2007; 7:2281–2290. [PubMed: 17645363]

45. Zlotnick A, Porterfield JZ, Wang JC. To build a virus on a nucleic Acid substrate. Biophys J. 2013; 104:1595–1604. [PubMed: 23561536]

46. Belyi VA, Muthukumar M. Electrostatic origin of the genome packing in viruses. Proc Natl Acad Sci U S A. 2006; 103:17174–17178. [PubMed: 17090672]

47. Hu Y, Zandi R, Anavitarte A, Knobler CM, Gelbart WM. Packaging of a polymer by a viral capsid: the interplay between polymer length and capsid size. Biophys J. 2008; 94:1428–1436. [PubMed: 17981893]

48. Ni P, Wang Z, Ma X, Das NC, Sokol P, Chiu W, Dragnea B, Hagan M, Kao CC. An examination of the electrostatic interactions between the N-terminal tail of the Brome Mosaic Virus coat protein and encapsidated RNAs. Journal of molecular biology. 2012; 419:284–300. [PubMed: 22472420]

49. Siber A, Podgornik R. Nonspecific interactions in spontaneous assembly of empty versus functional single-stranded RNA viruses. Phys Rev E Stat Nonlin Soft Matter Phys. 2008; 78:051915. [PubMed: 19113163]

50. Ting CL, Wu J, Wang ZG. Thermodynamic basis for the genome to capsid charge relationship in viral encapsidation. Proceedings of the National Academy of Sciences of the United States of America. 2011; 108:16986–16991. [PubMed: 21969546]

51. Mukherjee S, Abd-El-Latif M, Bronstein M, Ben-nun-Shaul O, Kler S, Oppenheim A. High cooperativity of the SV40 major capsid protein VP1 in virus assembly. PLoS One. 2007; 2:e765. [PubMed: 17712413]

52. Raillon C, Granjon P, Graf M, Steinbock LJ, Radenovic A. Fast and automatic processing of multi-level events in nanopore translocation experiments. Nanoscale. 2012; 4:4916–4924. [PubMed: 22786690]

53. Porterfield JZ, Zlotnick A. A simple and general method for determining the protein and nucleic acid content of viruses by UV absorbance. Virology. 2010; 407:281–288. [PubMed: 20850162]

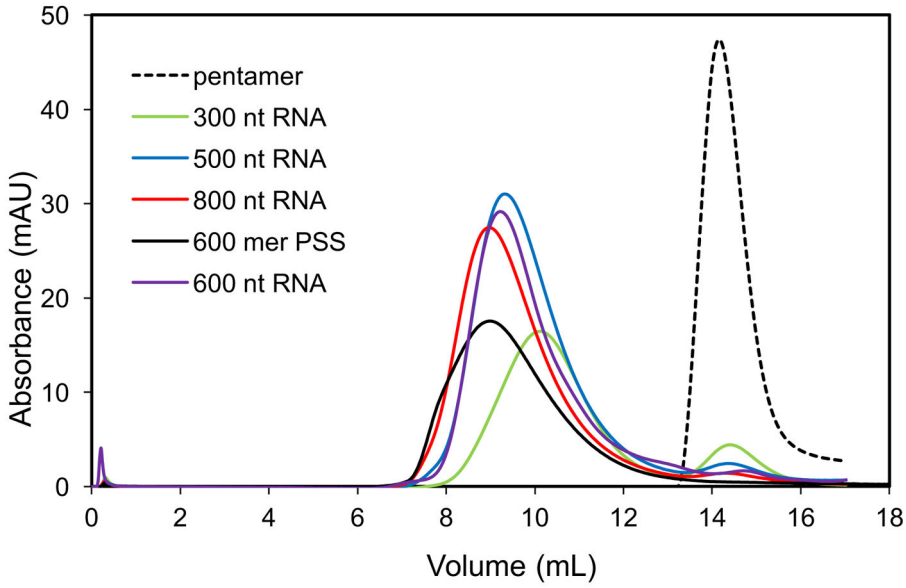


**Figure 1. Size exclusion chromatograms (SEC) of PSS and RNA assembly products**

The VP1 pentamer (dashed line) eluted at 14.3 mL. PSS assembly products (black) eluted at 9 mL with a shoulder around 7.9 mL. RNA assembly products for 300 nt (green), 500 nt (blue), 600 nt (purple), and 800 nt (red) RNAs eluted at 10.1, 9.3, 9.2, and 9 mL, respectively.

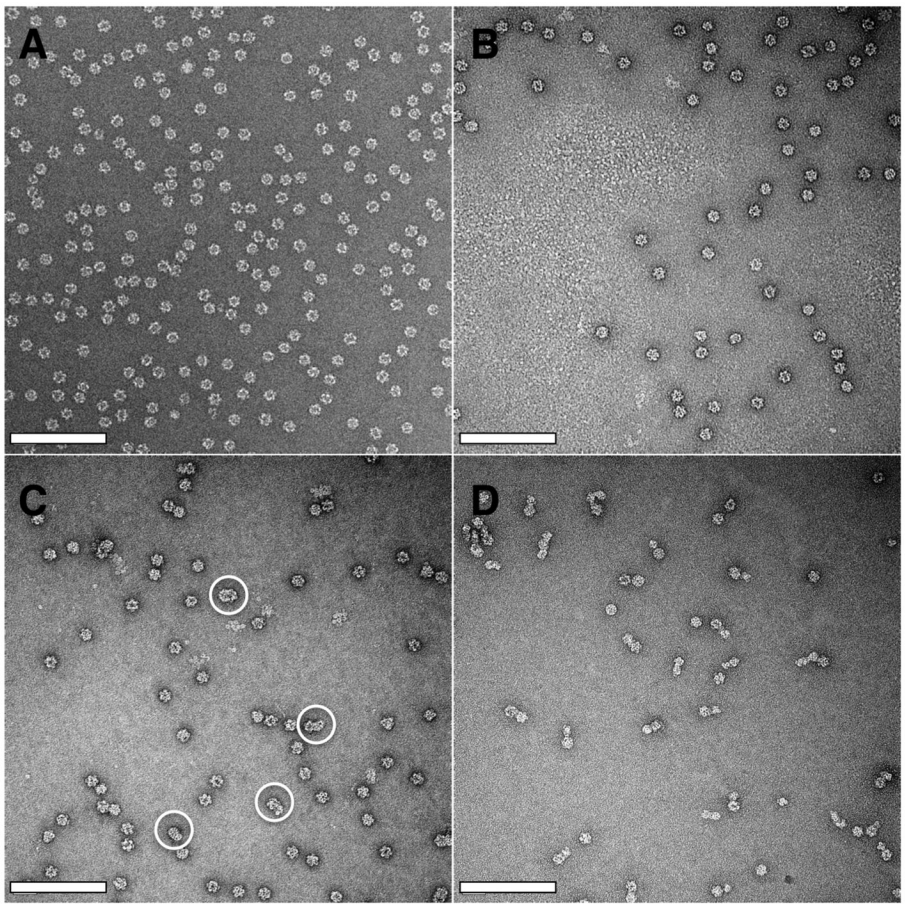


**Figure 2. Morphology of RNA and PSS assembly products by TEM**

(A) 300 nt RNA assembly products appear to be T=1 VLPs. (B) 500 nt RNA assembly products also appear to be T=1 VLPs. (C) 800 nt RNA assembly products show T=1 VLPs and oversized particles (white circles). (D) PSS assembly products show singlets, doublets, and triplets of T=1 size particles. The scale bars in all images are 200 nm wide and 22 nm high, the diameter of a T=1 VLP.

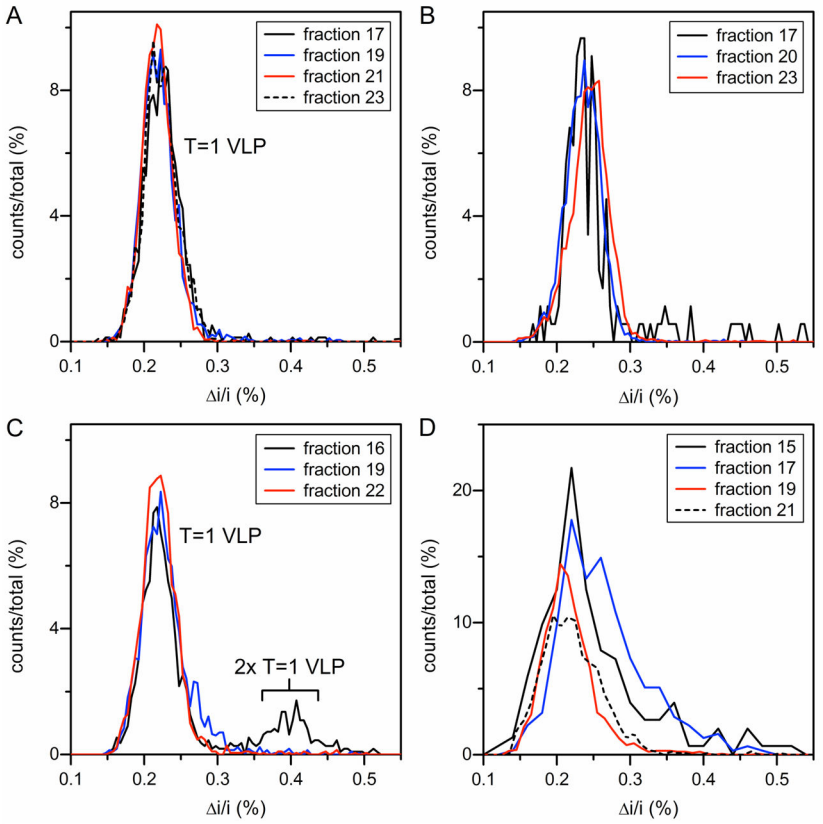


**Figure 3. Histograms of average pulse amplitude for products assembled from (A) 300 nt RNA, (B) 500 nt RNA, (C) 800 nt RNA, and (D) 600mer PSS and purified by SEC**

(A) All fractions of 300 nt RNA assembly products have similar average pulse amplitudes for T=1 VLPs, which indicate homogeneous assembly (total counts = 6831). (B) Most 500 nt RNA assembly products exhibit a single peak in pulse amplitude for T=1 VLPs, which suggests mostly homogeneous assembly and some larger species were detected in the earliest fraction (fraction 17; total counts = 6141); (C) The earliest fraction in 800 nt RNA assembly products (fraction 16) shows a significant number of pulses at nearly double the pulse amplitude of the T=1 VLP (total counts = 5358). (D) PSS assembly products show a range of pulse amplitudes with a significant number of larger species (total counts = 2654). The average pulse amplitude ($\Delta i$) is normalized by the baseline current (i).

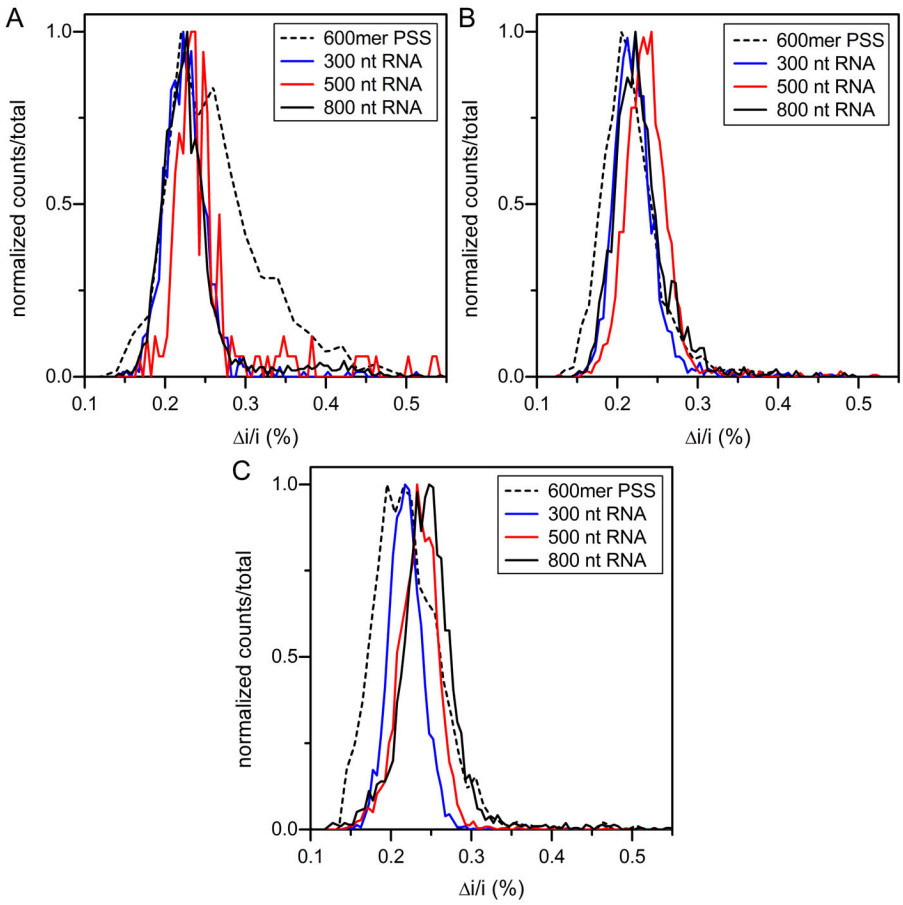


**Figure 4. Histograms of average pulse amplitude for assembly products from SEC fractions (A) 17, (B) 19, and (C) 21**

(A) Histograms for fraction 17 (total counts = 3749). The assembly becomes more heterogeneous as the size of the substrate increases. (B) Histograms for fraction 19 (total counts = 7479). The assembly is much more homogeneous, but the larger substrates still show some slight preference toward larger products. (C) Histograms for fraction 21 (total counts = 9606). The assembly is largely homogeneous, but the larger substrates shift slightly to larger species. The average pulse amplitude ($\Delta i$) is normalized by the baseline current ($i$).

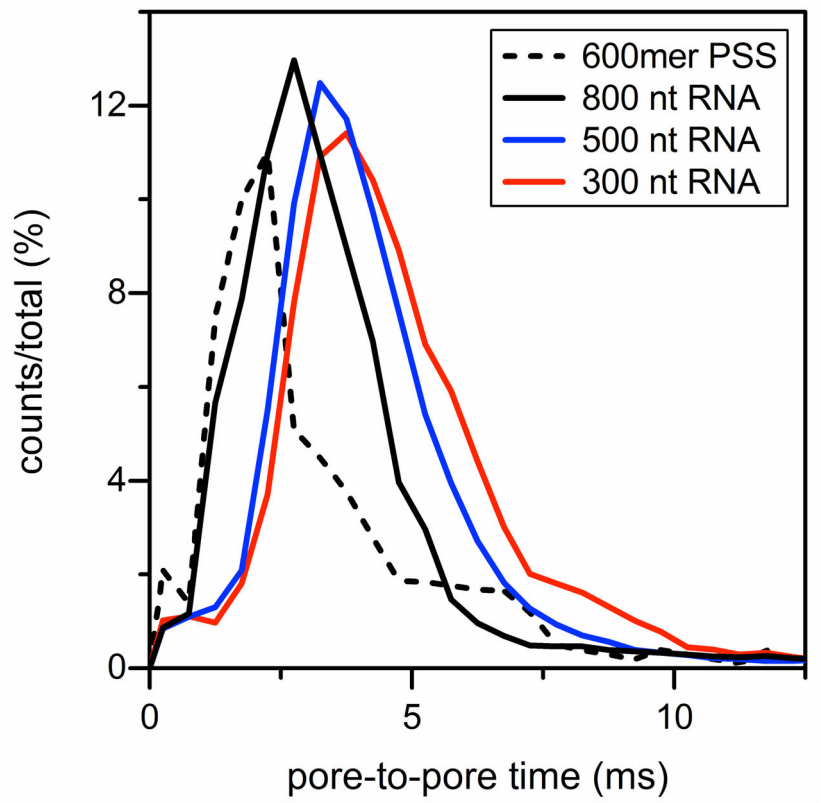


**Figure 5. Histograms of the pore-to pore times for products assembled with 300 nt RNA, 500 nt RNA, 800 nt RNA, and 600mer PSS and purified by SEC**

For the products assembled with RNA, pore-to-pore times decrease with increasing RNA length and, therefore, excess negative charge. Products assembled with PSS have the shortest pore-to-pore times, which suggests the PSS is not completely packaged in the VLPs. Assembly products were taken from fractions 19 and 20 (total counts = 20923).

**Table 1**

Distribution of Assembly Products by SEC.

| Substrate | % peak area | | % VP1 | | <RNA/capsid> |
|---|---|---|---|---|---|
| | capsid | pentamer | capsid | pentamer | |
| **300 nt RNA** | 85.5% | 14.5% | 77% | 23% | 1.30 |
| **500 nt RNA** | 96.1% | 3.9% | 94% | 6.2% | 1.07 |
| **600 nt RNA** | 96.1% | 3.9% | 94% | 6.2% | 1.07 |
| **800 nt RNA** | 96.5% | 3.5% | 94% | 5.6% | 1.06 |
| **600 mer PSS** | 1 | 0 | 100% | 0 | 1 |

Peak areas were calculated from the chromatographs in figure 1. The total absorbance of the capsid peak includes RNA absorbance with an estimated extinction coefficient of 4000 $M^{-1}$ $cm^{-1}$ per nucleotide [53]. PSS has negligible absorbance at 280 nm. Assuming all substrate was in the capsid peak, we calculated the fraction of VP1 in the free pentamer and capsid peaks.

## Table 2

Correlations of substrate length, 2nd structure, and charge ratio to the assembly products.

| Substrate | Charge ratio for T=1 | Product |
|---|---|---|
| **300 nt ssRNA** | 1 | T=1 |
| **500 nt ssRNA** | 1.67 | T=1 |
| **600 nt ssRNA** | 2 | T=1 |
| **800 nt ssRNA** | 2.67 | T=1 and oversized particles |
| **600 mer PSS** | 2* | Doublets, triplets, and T=1 |

For PSS reactions where the initial ratio of pentamers per polymer was 12:1, doublets and triplets comprised of one PSS and 24 or 36 pentamers would be neutral or undercharged with ratios of 1.0 and 0.67, respectively. Therefore, we cannot exclude the possibility that they contain more than one PSS molecule per complex.